Lasers in Manufacturing Conference 2023

LTT effect simulation by varying the Cr-Ni compositions in the weld zone during laser beam welding for high alloy steel and studying its influence on M_s temperature and residual stresses

Karthik Ravi*, Krishna Murthy[a,*], Akyel, Fatma[a], Olschok, Simon[a], Reisgen, Uwe[a]

[a]*Welding and Joining Institute, RWTH Aachen University, Aachen, Germany*

Abstract

The main objective of this work is to study and reduce the formation of residual stresses generated during laser beam welding. The reduction of residual stresses is achieved by introducing the effect of Low Transformation Temperature (LTT) in the weld. Commonly this effect is used in unalloyed steel, but in this study the effect is introduced in stainless steel by introducing an unalloyed filler wire. By varying the filler wire deposition and laser power, the Cr-Ni content can be varied (Cr varied between 13-15%). The thermo-metallurgical-mechanical simulation model is created by defining the initial phase fractions, mechanical constraints, and thermal-mechanical properties for different Cr-Ni compositions in the weld and the base metal. The computed Ms. temperature and strain rate variations for different Cr-Ni compositions are validated by dilatometer, and the residual stresses are validated by drill hole method, and optimum Cr-Ni composition is selected to achieve lower reduced residual stress.

Keywords: Numerical simulation; Residual stresses; LTT effect; Laser beam welding

1. Introduction

Laser Beam Welding (LBW) of high alloy plays a vital role in various industries due to the desirable combination of mechanical properties and corrosion resistance offered by these materials (Lebedev & Kosarchuk, 2000). However, during LBW, the material undergoes substantial thermal cycles, resulting in phase transformations and the development of residual stresses (Dilthey, 2005).In order to reduce this residual stress (RS), LTT effect is induced in the weld seam. The main role of this effect is to influence the martensite start (M_s) temperature.

The M_s temperature is the temperature at which austenite begins to transform into martensite and is accompanied by a significant amount of volumetric expansion, which can largely compensate for thermal shrinkage during the cooling stage of the welding process. The M_s temperature is influenced by the alloying elements present in the material composition, such as chromium (Cr) and nickel (Ni). These elements play a significant role in altering the phase transformation behavior and subsequent mechanical properties of the welded joint. By strategically modifying the Cr-Ni compositions in the weld zone, it is possible to tailor the M_s temperature and control the phase transformations, thereby influencing the resultant RS (Akyel et al., 2022a; Kromm, Dixneit, & Kannengiesser, 2014; Ramesh, Dinaharan, Ravikumar, & Akinlabi, 2020). In this study, a combined experimental and numerical simulation-based approaches have been employed. Experimental studies involve conducting LBW, Dilatometer analysis, chemical analysis and RS measurements. In parallel to this, numerical simulation is used to predict the RS by considering the thermo-metallurgical-mechanical effect for different Cr- Ni compositions in the weld seam.

2. Experiment and material

A high alloy steel sheet (1.4301/AISI 304) with dimension of 100x50x5 mm was welded at the center of the plate with LBW process in a single pass with full penetration. In order to achieve the LTT effect, dissimilar weld is performed by introducing the low alloy filler material G3Si1(EN ISO 14,341-A G 42 5 M21 3Si1/ AWS A5.18:ER70S-6) by the company Fliess, Germany, into the weld seam. Thus, the Cr and Ni alloying content of the base material is reduced. The chemical composition of both base material and the filler material is mentioned in the Table *1* (Akyel et al., 2022a)**.**

Table 1. Chemical composition for Base material (1.4301) and filler material (G3Si1)

Material	Fe	C	Si	Mn	Cr	Ni	Mo
1.4301	70.7	0.02	0.42	1.68	18.2	8.24	0.036
G3Si1	97.3	0.07	0.86	1.44	0.045	0.019	0.008

Along with the introduction of low alloy filler material into the base material to achieve different Cr-Ni compositions (in this study, Cr composition is varied between 13% to 15%) in the weld seam, the weld seam width, height and welding parameters has been varied and the same has been listed in the *Table* 2.

Table 2. Welding parameter and weld seam dimension to achieve different Cr %

				Oscillation parameter			Seam Preparation		
Name	Power P[kW]	Weld speed V_w [m/min]	Feed Speed V_f [m/min]	Frequency F [Hz]	Amplitude [%]	Figure [-]	Width W [mm]	Depth D [mm]	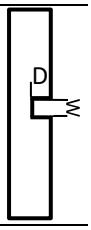
LTT-Cr-13	6	0.8	6.9	150	3	Sine	1.4	1.4	
LTT-Cr-14	5.8	0.8	3.4	150	5	Sine	1.6	1.0	
LTT-Cr-15	5.8	0.8	3.4	150	5	Sine	1.4	1.0	

The welding test were performed using a LBW process. The beam was generated using a Trumpf TruDisk 16002 disk laser, which has a maximum beam power of 16 kW and a fiber diameter of 400 µm was used to transport the beam with an optic aspect ratio of 1:3. With this arrangement, a focal diameter of 1200 µm was achieved on the surface of the weld plate. The focal diameter was wide enough to melt the cold filler wire as well as base material, so that a de-alloying of the high alloy base material occurred. Furthermore, a scanner for oscillation was used which further helped with the homogeneous mixing of the base and filler material and ensured wider weld seam in the upper area of the weld seam. The filler wire was introduced with a Mini Drive feeding system developed by the Welding and Joining Institute of RWTH Aachen Fig. 1(a). The inclination angle was set to 45◦. This process is described in previous works of the authors (Akyel et al., 2022a; Akyel et al., 2022b; Krishna Murthy, Akyel, Reisgen, & Olschok, 2022). The temperature distribution in the specimen is recorded with type K thermocouples that were tacked on the top of the component. The distance between each thermocouple was 4 mm and 8mm from the weld seam. The Fig. 1 (c); (d); (e) is the weld seam cross-sections for different Cr% in the weld seam and this was produced by using the parameters from the *Table* 2.

The dilatometer test was performed to determine the M_s and M_f temperatures and the corresponding strain rate for the selected range of chromium compositions. The samples were prepared so that the chromium compositions were 13%, 14%, and 15%, respectively. This was achieved by melting a selected amount of base and filler material in an electric arc furnace (arc furnace MAM-1, Edmund Bühler GmbH) and then verified by OES analysis. Later, these melted samples were turned into a hollow cylindrical bar with a length of 8 mm and a diameter of 4 mm (with a wall thickness of 1 mm) according to the specification of ASTM standard A 1033-18 (A1003, 2018).

The RS built up during welding process was measured using the hole drilling method (ESPI- Electronic speckle pattern interferometry). A drill with a diameter of 0.8 mm was used and the measurements were carried out at the depth of 0.50 mm. The measurement was taken every 10 mm in the longitudinal direction at the weld in the welding direction starting from 20 mm to 80 mm and every 5 mm in transversal direction (perpendicular) to the weld up to 15 mm (Krishna Murthy et al., 2022).

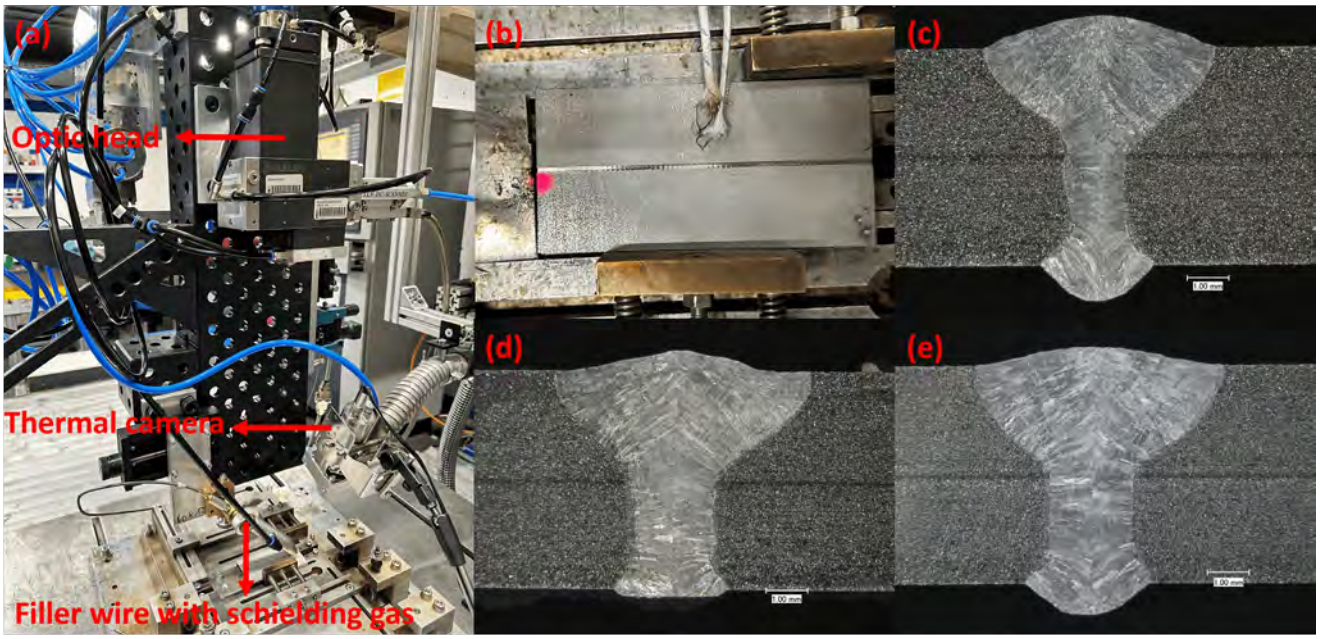

Fig. 1. (a) Welding setup at Welding and Joining Institute of RWTH Aachen*;* (b) *Workpiece with* thermocouple; (*c*) Weld cross section for Cr 13%; (*d*) Weld cross section for Cr 14%; (*e*) Weld cross section for Cr 15%

3. Simulation method

The LBW process was numerically computed using a commercial FEA solver Abaqus. In this numerical simulation model, symmetric modelling technique was implied in order to reduce the computational time. Along with that, the model was meshed fine only in the area of interest (AOI).

In LBW, the AOI is weld seam and heat affected zone. The rest of the model is meshed by coarse mesh. The simulation approach that has been implemented in this work to predict the RS with LTT effect for different Cr-Ni compositions has been described by a flow chart Fig. 2.

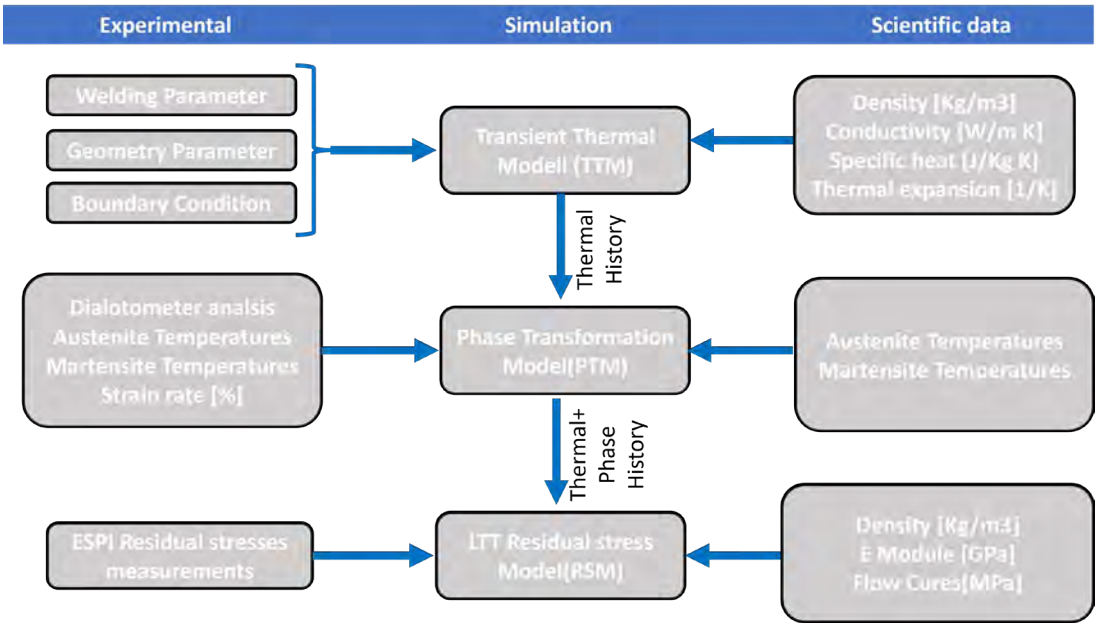

Fig. 2. Simulation flow chart to predict the RS with LTT effect for different Cr-Ni compositions

The transient thermal model (TTM) is computed based on the input of the welding parameter, geometry parameter, boundary conditions and thermomechanical properties with varying temperatures. In this study the geometry parameter is considered as a rectangle plate with a dimension corresponding to 100 x 25 x 5 mm. The welding parameter gives the information about the amount of heat that has to be inputted into the numerical model and the welding velocity Table 2.In TTM, the boundary conditions used are convection and radiation, where the numerical model is cooled down to room temperature without any forced convection. To calculate the thermomechanical properties, chemical compositions of the weld seam and base material is required. These chemical compositions of the weld seam for different Cr-Ni compositions that was welded using the parameters from Table 2 is calculated using Energy-dispersive X-ray spectroscopy. The below table shows the chemical compositions for all 3 cases Table *3*.

Table 3. Chemical composition for Base material (1.4301) and filler material (G3Si1) for different Cr-Ni compositions

Material in weld seam	Fe	Si	Mn	Cr	Ni
LTT-Cr-13 %	79.638	0.450	1.326	12.936	5.647
LTT-Cr-14 %	77.421	0.455	1.463	14.575	6.084
LTT-Cr-15 %	76.171	0.413	1.399	15.173	6.845

Using these compositions from Table *3* , the thermomechanical properties with varying temperature is calculated using JMat Pro (SAUNDERS, N., et al., 2003). The heat source model in the TTM is incorporated from the previous work (Akyel, Reisgen, Olschok, & Murthy, 2021), where the mesh density is fine in the weld zone and heat affect zone and it gets coarser with the increase in distance from the weld seam. In TTM, a linear heat transfer brick element with eight nodes (DC3D8) with a total number of 28886 nodes and 25000 elements was used. The volumetric heat load (heat source) was applied on the symmetry edge using a subroutine called DFLUX.

The phase transformation is computed based on the thermal history of the TTM. Using this temperature history, the computation of phase fractions has been divided into two cycles.

(a) Heating cycle: austenite undergoes phase transformation and the austenitic transformation kinetic computed using Avrami numerical equation (*1*) (Winczek & Skrzypczak, 2016).

$$V_A = V_{in} * \left(1 - \exp\left[-b_j t(T)^{n_j}\right]\right) \quad (1)$$

Where, V_A : Austenite phase fraction; T : Current temperature; A_1 : Austenization temperature;

A_3:Transformation finish temperature; V_{in}: Initial phase fraction

(b) Cooling cycle: As the cooling cycle is quick, the austenite undergoes martensitic transformation along with the possibility of ferrite and residues of austenite. For this purpose, the kinetics of ferritic and residues of austenitic transformation is computed using Johnson-Mehl-Avrami numerical equation (*2*) (Winczek & Skrzypczak, 2016).

$$V_j = V_\gamma * V_j^{max} * \left(1 - \exp\left[-b_j (T)^{n_j}\right]\right) \quad (2)$$

Where,

$$n_j = \left[\ln\left(\ln\left(1 - V_j^s\right)\right)/\ln\left(1 - V_j^f\right)/\ln\left(T_j^s/T_j^f\right)\right],\ b_j = n_j\left(1 - V_j^f\right)/T_j^s$$

T_j^s/T_j^f: Starting and end transformation temperature.

V_j^s/V_j^f: Starting and end phase fraction

Martensitic transformation was realised using and Koistinen-Marburger numerical equation (*3*) (Deng, 2009). Where the material constant b was assumed to be 0.0185 and the Martensite start temperature was calculated from the (*4*) and (*5*) (Wang, Woo, Kim, Em, & Lee, 2018).

$$V_m = V_\gamma(1 - \exp[-b(M_s - T)]) \quad (3)$$

$$M_s = 948,.21 - 448.5C - 3.75Si - 28.53Mn - 38.8Ni - 39.50Cr - 14.3Mo \quad \text{For } M_s < 200\ °C \quad (4)$$

$$M_s = 600.92 - 448.5C - 3.75Si - 35.64Mn - 20.46Ni - 13.70Cr - 14.3Mo \quad \text{For } M_s > 200\ °C \quad (5)$$

Residual stresses is a combination of thermal, mechanical, and metallurgical effect. The developments of strain in heating and cooling cycle was implemented from the authors previous work (Krishna Murthy et al., 2022) and are computed using a UEXPAN subroutine in which solution dependent variables SDV's will be used to output the phase fractions. Along with this, the strain rates that was obtained from the dilatometer for each phase was integrated in the subroutine Fig. 5.

4. Results and Discussion

The experimental and computed numerical simulation results for different Cr-Ni composition in the weld seam will be discussed and at the same time the simulation model will also be validated with the experimental. The effect of different Cr-Ni compositions on the martensite start temperature and its influence on the residual stresses will be discussed.

4.1. Transient temperature model

The thermal simulation model is validated using the measured temperature from the thermo couples during the welding and its respective weld cross sections are compared with the computed TTM. For each Cr-Ni composition a TTM was created in which the material compositions and the thermal material properties for each case was varied. The thermal properties that were calculated using JMat-Pro was based on the chemical compositions which was listed in the Table *3* and for the base material from Table 1.

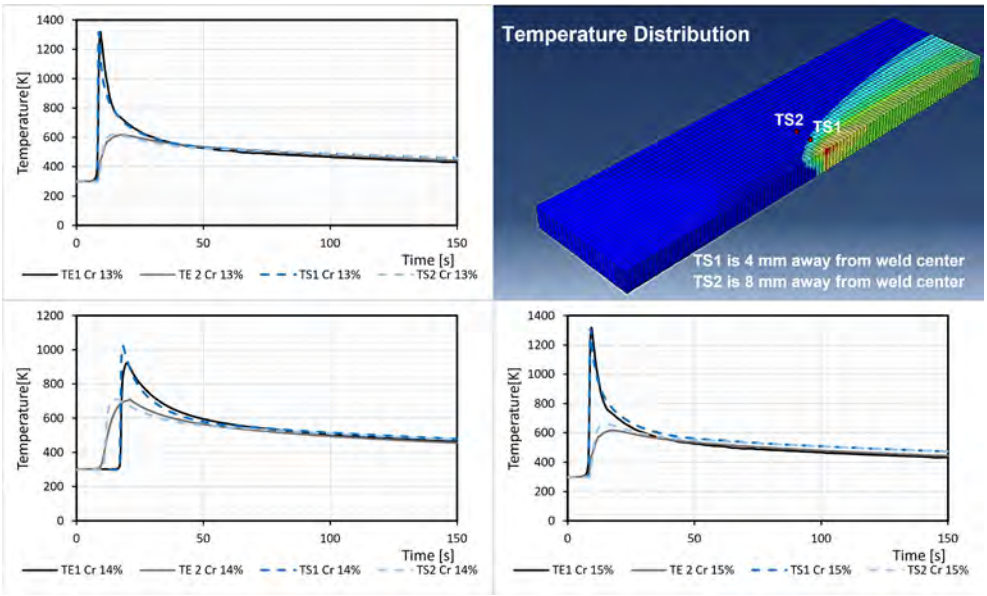

Fig. 3. Experimental and Simulation temperature distribution comparison

The temperature measured position (that is 4 and 8 mm away from the center of the weld seam) for both simulation and experimental were kept same. From the plotted graphs for each case, the temperature curves have a very good agreement (approximately 90 % and above) in both heating and cooling cycle Fig. 3.

This ensures that the computed temperature distribution in the simulated workpiece is matching the experimental temperature results.

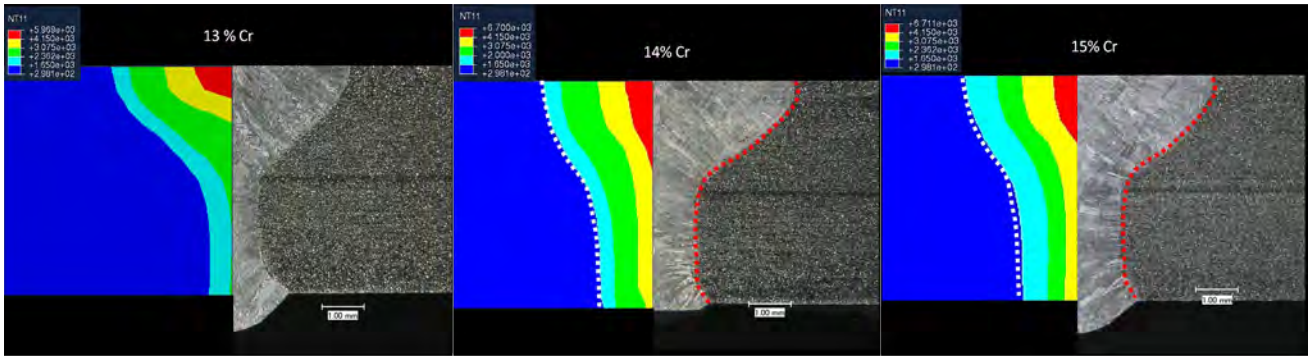

Fig. 4. Experimental and Simulation weld geometry cross section comparison

The heat that has been inputted into the numerical simulation model and the computed numerical weld seam geometry cross-section has been verified using the weld macroscopic cross-section for all the three cases Fig. 4. From these comparisons, it can be said that the TTM is accurate enough and this temperature distribution can be further used as a thermal history for computing the phase fractions and residual stresses.

4.2. Phase transformation model (PTM)

The thermal history from the TTM is used to compute the kinetics of phase transformation in both heating and cooling weld cycle. In all cases, only cooling cycle has been discussed as the resulting transformation will have more influence on the building of RS. From the PTM, for 13 %, 14 % and 15% of chrome in the weld seam has been tabulated below Table 4. The start and finish of martensite is calculated from the dilatometry curve Fig. 5.

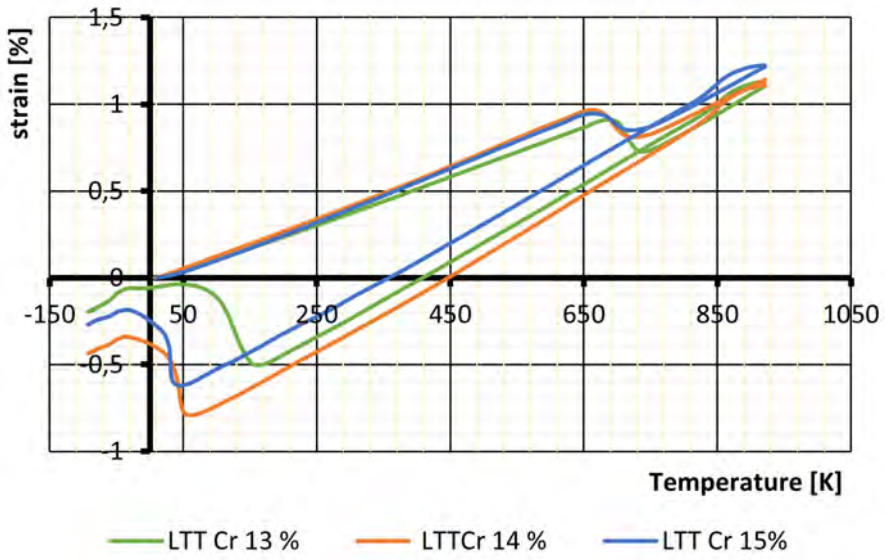

Fig. 5. Dilatometer strain versus temperature curves for different Cr compositions

Table 4. Computed phase fractions and Martensite temperatures (Ms and Mf)

Material in weld seam	Austenite [%]	Ferrite [%]	Martensite [%]	M_s [°C]	M_f [°C]
LTT-Cr-13 %	23.01	4.54	72.41	160.70	50.99
LTT-Cr-14 %	63.23	4.98	32.79	70.52	-33.97
LTT-Cr-15 %	73.98	9.87	16.14	33.97	-45.33

Based on the M_s temperature from the dilatometry, it can be said that the computed phase fractions are nearly matching. But the verification of phase transformation model has be made using other methods (Gómez, Medina, & Caruana, 2003). This is carried out in the further studies.

4.3. Residual stress model (RSM)

The RSM for all the three cases is validated with the ESPI RS measurement. The distribution of RS in the weld was strongly influenced by the Cr-Ni compositions The welded samples for all the three different cases were used to measure the RS on the weld seam. The measurement was recorded at 0.5 mm depth and at the same depth the simulated RS was also recorded and compared.

From the Fig. 6, the predicted (computed) RS and measured RS also had good agreement in all three cases.

(a) LTT-Cr-13 %: In this case, the martensite temperature starts at 160.7 °C and finishes at 50.99 °C, which means the martensitic transformation is completed before room temperature. This leads to a greater volume expansion and thus compressive stress is induced in the weld seam. For this reason, it can be seen in the graph for 13 % chrome, compressive longitudinal stress has been seen.
(b) LTT-Cr-14 %: In this case, the martensite temperature starts at 70.52 °C and finishes at -33.97 °C, which means the martensitic transformation is much less. Therefore, not much compressive stress can be seen in the weld seam.
(c) LTT-Cr-15 %: In this case, the martensite temperature starts at 33.97 °C, which means the martensitic transformation cannot be achieved. Therefore, the stresses spike up in the weld seam.

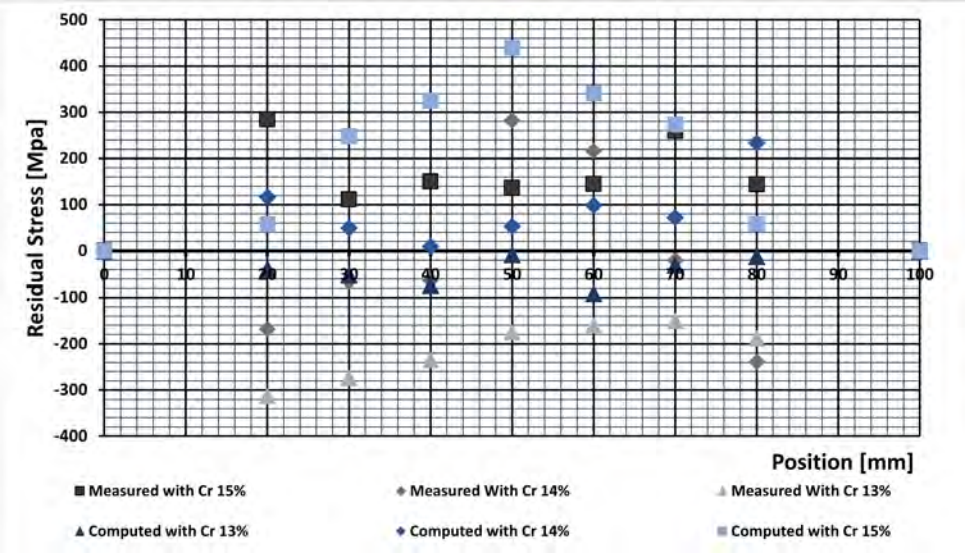

Fig. 6. Experimental and simulation Residual stress comparison

5. Summary

The results obtained from the simulation provide valuable insight into the effects of different Cr-Ni compositions on LLT behaviour and RS during laser beam welding of high alloy steel. The relationship between alloy composition, phase transformation kinetics and mechanical properties was analysed for each case. It was found that a chromium content of 13% in the weld results in a good LLT effect, as shown by dilatometry analysis, measurement of RS and RSM. This was mainly because the martensite transformation was fully achieved, resulting in a reduction of RS in the weld. In contrast, complete martensite transformation was not achieved for the other two compositions. The predicted RS agreed with the trend of experimentally measured RS, but not in terms of magnitude. This could be due to the error factor from the calculated phase fractions and other material constants. To obtain an accurate RS prediction model, the RSM needs to be further optimised and also the verification of the predicted phase fractions needs to be done. This is planned in the further work together with the numerical modelling to predict the distortion with LTT effect.

Acknowledgements

The presented investigations were carried out at RWTH Aachen University Welding and Joining Institute ISF within the framework of the Collaborative Research Centre SFB1120-236616214 “Bauteilpräzision durch Beherrschung von Schmelze und Erstarrung in Produktionsprozessen” and funded by the Deutsche Forschungsgemeinschaft e.V. (DFG, German Research Foundation). The sponsorship and support is gratefully acknowledged.

Simulations were performed with computing resources granted by RWTH Aachen University under project rwth1256.

Reference

A1003 (2018). *A01 Committee. Practice for Quantitative Measurement and Reporting of Hypoeutectoid Carbon and Low-Alloy Steel Phase Transformations; ASTM International: West Conshohocken, PA, USA, 2018.*

Akyel, F., Gamerdinger, M., Olschok, S., Reisgen, U., Schwedt, A., & Mayer, J. (2022a). Adjustment of chemical composition with dissimilar filler wire in 1.4301 austenitic stainless steel to influence residual stress in laser beam welds. *Journal of Advanced Joining Processes, 5*, 100081.

Akyel, F., Gamerdinger, M., Olschok, S., Reisgen, U., Schwedt, A., & Mayer, J. (2022b). Residual Stress Reduction with the LTT Effect in Low Carbon Manganese-Steel through Chemical Composition Manipulation Using Dissimilar Filler Material in Laser Beam Welding. *Metals, 12*(6), 911.

Akyel, F., Reisgen, U., Olschok, S., & Murthy, K. (2021). Simulation of Phase Transformation and Residual Stress of Low Alloy Steel in Laser Beam Welding. In U. Reisgen, D. Drummer, & H. Marschall (Eds.), *Lecture Notes in Mechanical Engineering. Enhanced Material, Parts Optimization and Process Intensification* (pp. 3–13). Cham: Springer International Publishing.

Deng, D. (2009). FEM prediction of welding residual stress and distortion in carbon steel considering phase transformation effects. *Materials & Design, 30*(2), 359–366.

Dilthey, U. (2005). *Schweißtechnische Fertigungsverfahren 2: Verhalten der Werkstoffe beim Schweißen* (3., bearbeitete Auflage). *SpringerLink Bücher.* Berlin, Heidelberg: Springer Berlin Heidelberg.

Gómez, M., Medina, S. F., & Caruana, G. (2003). Modelling of Phase Transformation Kinetics by Correction of Dilatometry Results for a Ferritic Nb-microalloyed Steel. *ISIJ International, 43*(8), 1228–1237.

Krishna Murthy, K. R., Akyel, F., Reisgen, U., & Olschok, S. (2022). Simulation of transient heat transfer and phase transformation in laser beam welding for low alloy steel and studying its influences on the welding residual stresses. *Journal of Advanced Joining Processes, 5*, 100080.

Kromm, A., Dixneit, J., & Kannengiesser, T. (2014). Residual stress engineering by low transformation temperature alloys—state of the art and recent developments. *Welding in the World, 58*(5), 729–741.

Lebedev, A. A., & Kosarchuk, V. V. (2000). Influence of phase transformations on the mechanical properties of austenitic stainless steels. *International Journal of Plasticity, 16*(7-8), 749–767.

Ramesh, R., Dinaharan, I., Ravikumar, R., & Akinlabi, E. T. (2020). Microstructural characterization and tensile behavior of Nd:YAG laser beam welded thin high strength low alloy steel sheets. *Materials Science and Engineering: A, 780*, 139178.

SAUNDERS, N., et al. (2003). Using JMatPro to model materials properties and behavior. Jom, 2003, 55. Jg., S. 60-65., *Jg., S. 60-65.*

Wang, H., Woo, W., Kim, D.-K., Em, V., & Lee, S. Y. (2018). Effect of chemical dilution and the number of weld layers on residual stresses in a multi-pass low-transformation-temperature weld. *Materials & Design, 160*, 384–394.

Winczek, J., & Skrzypczak, T. (2016). Thermomechanical States in Arc Weld Surfaced Steel Elements. *Archives of Metallurgy and Materials, 61*(3), 1623–1634.